REPORT DOCUMENTATION PAGE

AFRL-SR-AR-TR-04-

88

0136

The public reporting burden for this collection of information is estimated to average 1 hour per res ~~isting data sources,~~
gathering and maintaining the data needed, and completing and reviewing the collection of information ~~act of this collection~~
of information, including suggestions for reducing the burden, to Department of Defense, Wast ~~ations and Reports~~
(0704-0188), 1215 Jefferson Davis Highway, Suite 1204, Arlington, VA 22202-4302. Respondent: ~~, no person shall be~~
subject to any penalty for failing to comply with a collection of information if it does not display a curr
PLEASE DO NOT RETURN YOUR FORM TO THE ABOVE ADDRESS.

1. REPORT DATE *(DD-MM-YYYY)*	2. REPORT TYPE Final	3. DATES COVERED *(From - To)* 15 Nov 99 - 14 Nov 02

4. TITLE AND SUBTITLE
Instabilities and Transition in Three-Dimensional Boundary Layers, with emphasis on Gas-Turbine-Blade Flows

5a. CONTRACT NUMBER

5b. GRANT NUMBER
F49620-00-1-0066

5c. PROGRAM ELEMENT NUMBER

6. AUTHOR(S)
Oleg S. Ryzhov

5d. PROJECT NUMBER

5e. TASK NUMBER

5f. WORK UNIT NUMBER

7. PERFORMING ORGANIZATION NAME(S) AND ADDRESS(ES)

University Of California, Davis
One Shields Avenue
Davis, CA 95616

8. PERFORMING ORGANIZATION REPORT NUMBER

9. SPONSORING/MONITORING AGENCY NAME(S) AND ADDRESS(ES)

AFOSR/NM
4015 Wilson Blvd., Room 713
Arlington, VA 22203-1954

10. SPONSOR/MONITOR'S ACRONYM(S)

11. SPONSOR/MONITOR'S REPORT NUMBER(S)

12. DISTRIBUTION/AVAILABILITY STATEMENT

Approved for Public Release; Distribution Unlimited

13. SUPPLEMENTARY NOTES

20040305 026

14. ABSTRACT
Absolute instability of (Gortler vortices on the severely curved concave pressure side of a gas-turbine blade is the main thrust of the third-year work under this grant. For the most part, the Gortler vortices have been investigated in an incompressible boundary layer over thin-wing sections or artificial inserts on an otherwise flat plate. The cascade of modern aircraft engines operate in the high subsonic Mach number regime with velocity fields strongly affected by centrifugal forces maintained by the large curvature of profiles. Unsteady spiral-type vortices developing in these environments provoke the absolute instability in the streamwise direction of the boundary layer leading to earlier transition. An effort undertaken after the meeting in Shalimar (May 29-31, 2002) show that the heat transfer coefficient is even more susceptible to enhancing oscillations in the upstream moving wave packets than the pressure.

15. SUBJECT TERMS

16. SECURITY CLASSIFICATION OF:			17. LIMITATION OF ABSTRACT	18. NUMBER OF PAGES	19a. NAME OF RESPONSIBLE PERSON Dr. Oleg S. Ryzhov
a. REPORT	b. ABSTRACT	c. THIS PAGE			

19b. TELEPHONE NUMBER *(Include area code)*
530-752-0580

Standard Form 298 (Rev. 8/98)
Prescribed by ANSI Std. Z39.18

Final Report on Research on
Instabilities and Transition in Three-Dimensional Boundary Layers,
with emphasis on Gas-Turbine-Blade Flows

Oleg S. Ryzhov

University of California, Davis

Introduction

Absolute instability of G̅rtler vortices on the severely curved concave pressure side of a gas-turbine blade is the main thrust of the third-year work under this grant. For the most part, the G̅rtler vortices have been investigated in an incompressible boundary layer over thin-wing sections or artificial inserts on an otherwise flat plate. The cascade of modern aircraft engines operate in the high subsonic Mach number regime with velocity fields strongly affected by centrifugal forces maintained by the large curvature of profiles. Unsteady spiral-type vortices developing in these environments provoke the absolute instability in the streamwise direction of the boundary layer leading to earlier transition. An effort undertaken after the meeting in Shalimar (May 29-31, 2002) show that the heat transfer coefficient is even more susceptible to enhancing oscillations in the upstream moving wave packets than the pressure.

The essence of the matter

The shape of a blade in broad use in the modern gas-turbine engines is shown in Figure 1. The concave pressure side is exposed to severe loading that can cause bad damages (spallation of thermal barrier coatings). The large curvature of the concave pressure side maintains centrifugal forces giving rise to G̅rtler vortices which make the problem all the more acute. The interaction of Tollmien-Schlichting waves and unsteady spiral-type vortical disturbances results in upstream-advancing wave packets that are at the heart of absolute instability in the streamwise direction of the oncoming flow. This kind of instability was discovered by Ryzhov (2001) in incompressible boundary layers and recently proved by Ryzhov & Bogdanova-Ryzhova (2002) to exist in the high subsonic Mach number regime. Surprisingly enough, temperature pulsations in the upstream-moving wave packets appear to have even larger amplitude than the pressure if the characteristic length of G̅rtler vortices grows without bound. The heat transfer coefficient also increases with the vortex length (Ryzhov & Bogdanova-Ryzhova, 2003). The temperature disturbances are triggered by the pressure and velocity fields that need to be evaluated first.

Conventional View of the G̅rtler instability mechanism

Typically, the G̅rtler vortices are thought of as steady disturbances having no characteristic length in the streamwise direction (Saric, 1994). Figure 2 illustrates this

conventional point of view under the tacit assumption of incompressible flow. Theoretically, an appropriate representation of velocity components reads

$$u(x,y,z) = U(x,y) + u(y)e^{\beta x} \cos(2\pi z/\lambda_z) \tag{1a}$$

$$v(x,y,z) = V(x,y) + v(y)e^{\beta x} \cos(2\pi z/\lambda_z) \tag{1b}$$

$$w(x,y,z) = w(y)e^{\beta x} \sin(2\pi z/\lambda_z) \tag{1c}$$

Here, the real exponent β determines the disturbance amplification rate in the streamwise direction, but there is no reference wavelength in this direction. The reference wavelength, λ_z, is specified only in the spanwise direction. It can be shown that stability properties of the boundary layer on a concave wall depend on a parameter

$$\overline{G} = \kappa \, \mathbf{Re} \tag{2}$$

called the Görtler number that incorporates the surface curvature κ and the Reynolds number $\mathbf{Re} \gg 1$. A number of other parameters enter the problem posed for compressible flow. The steady Görtler vortices do not disturb the boundary layer upstream of an external agency.

Unsteady Görtler vortices

Unsteady spiral-type vortical disturbances have been recorded many years ago in a related (incompressible) flow in a gap between two co-axial cylinders, one of which rotates and the other is at rest. The spiral-type vortices create a wavy motion shown in Figure 3 as applied to the problem of interest on the boundary layer developing on a concave solid surface. Here λ stands for the wavelength in the spanwise direction, however a characteristic wavelength is clearly seen to form in the disturbance pattern also in the direction of the oncoming stream.

The problem has been attacked theoretically by Denier, Hall & Seddougui (1991) who identified five different regimes inherent in the high-Reynolds number flow. Starting from the results of this paper, Choudhari, Hall & Streett (1994), arrived at a wrong conclusion that no upstream influence results from the viscous / inviscid interaction controlled by centrifugal forces. As a matter of fact, the first experimental evidence of upstream influence exerted by the vortical disturbances on a concave surface can be traced back to much earlier work by Mangalam, Dagenhart, Hepner & Meyers (1985).

An extended version of the triple-deck scheme

An asymptotic approach based on the assumption that the Reynolds number takes on sufficiently large values is required to resolve this controversy. The triple-deck theory offers a clue to start mathematical treatment. However, the classical version of the theory is based on the scaling intrinsic to Tollmien-Schlichting waves (Smith, 1979; Zhuk & Ryzhov, 1980). Vortical eigenmodes are not covered by this scaling and therefore fall beyond the Tollmien-Schlichting spectrum of frequencies. Neglect of centrifugal forces

maintained by the surface curvature is the decisive factor missing from the classical triple-deck analysis of wave motion. Higher order terms have to be retained in the asymptotic expansions to account for the curvature effects giving rise to Görtler vortical eigenmodes.

Guided by this preliminary consideration we introduce the time-space scaling

$$t^* = \varepsilon^2 \frac{L^*}{U_\infty^*} t, \quad x^* = L^*\left(1 + \varepsilon^3 x\right), \quad z^* = \varepsilon^3 L^* z \tag{3}$$

typical of the Tollmien-Schlichting spectral range fixed in terms of a small parameter

$$\varepsilon = \mathbf{Re}^{-\frac{1}{8}} \tag{4}$$

for $\mathbf{Re} \gg 1$. The definition of the normal-to-wall distance depends on a specific sublayer.

The Prandtl variable y_2 furnishes a pertinent scaling

$$y^* = \varepsilon^4 L^* y_2 \tag{5}$$

for most of the boundary layer where the desired functions have the following asymptotic expansions

$$\frac{u^*}{U_\infty^*} = u_2 = U_0(y_2) + \varepsilon u_{21}(t,x,y_2,z) + \ldots + \varepsilon^4 u_{24}(t,x,y_2,z) + \ldots \tag{6a}$$

$$\frac{v^*}{U_\infty^*} = v_2 = \varepsilon^2 v_{21}(t,x,y_2,z) + \ldots + \varepsilon^5 v_{24}(t,x,y_2,z) + \ldots \tag{6b}$$

$$\frac{w^*}{U_\infty^*} = w_2 = \varepsilon^2 w_{21}(t,x,y_2,z) + \ldots + \varepsilon^5 w_{24}(t,x,y_2,z) + \ldots \tag{6c}$$

$$\frac{p^* - p_\infty^*}{\rho_\infty^* U_\infty^{*2}} = p_2 = \varepsilon^2 p_{21}(t,x,y_2,z) + \ldots + \varepsilon^4 p_{23}(t,x,y_2,z) + \varepsilon^5 p_{24}(t,x,y_2,z) + \ldots \tag{6d}$$

$$\frac{\rho^*}{\rho_\infty^*} = \rho_2 = R_0(y_2) + \varepsilon \rho_{21}(t,x,y_2,z) + \ldots + \varepsilon^4 \rho_{24}(t,x,y_2,z) + \ldots \tag{6e}$$

The initial velocity and density profiles in the unperturbed boundary layer on the concave side of a blade are given by the leading-order terms $U_0(y_2)$ and $R_0(y_2)$ in (6a) and (6e), respectively. Logarithmic terms are not explicitly indicated since they have nothing to do with the instability problem in question. The scaling of the velocity, pressure and density fields comes from the classical triple-deck analysis providing the opening stage of the present study.

Based on the ideas set forth at the beginning of this report, let us focus on the pressure variations across the boundary layer which are balanced out by centrifugal

forces supported by the blade surface bending. Let $p_2^{(\kappa)}$ designate the contribution to the pressure from the curvature effects. Then

$$p_2^{(\kappa)} = \varepsilon^4\left[p_{23}^{(\kappa)}(x,y_2) + \varepsilon p_{24}^{(\kappa)}(t,x,y_2,z) + \ldots\right] \tag{7}$$

According to the classical boundary-layer theory by Prandtl,

$$\frac{\partial p_2^{(\kappa)}}{\partial y_2} = -\frac{\kappa}{\sqrt{\text{Re}}}\rho_2 u_2^2$$
$$= -\varepsilon^4\kappa\left\{R_0(y_2)U_0^2(y_2) + \varepsilon\left[2R_0(y_2)U_0(y_2)u_{21}(t,x,y_2,z) + U_0^2(y_2)\rho_{21}(t,x,y_2,z)\right] + \ldots\right\} \tag{8}$$

Hence

$$\frac{\partial p_{23}^{(\kappa)}}{\partial y_2} = -\kappa R_0(y_2)U_0^2(y_2) \tag{9}$$

is the pressure gradient in the initially unperturbed flow and

$$\frac{\partial p_{24}^{(\kappa)}}{\partial y_2} = -\kappa\left[2R_0(y_2)U_0(y_2)u_{21}(t,x,y_2,z) + U_0^2(y_2)\rho_{21}(t,x,y_2,z)\right] \tag{10}$$

determines the self-induced pressure oscillations responsible for the boundary-layer instability provoked by centrifugal forces.

To evaluate the last term giving the $O(\varepsilon^5)$-contribution to the pressure we need only the first-order solution for velocity components and density. This solution can be explicitly expressed in the form

$$u_{21} = A(t,x,z)\frac{dU_0}{dy_2} \tag{11a}$$

$$v_{21} = -\frac{\partial A(t,x,z)}{\partial x}U_0(y_2) \tag{11b}$$

$$R_0(y_2)U_0(y_2)\frac{\partial w_{21}}{\partial x} = -\frac{\partial p_{21}}{\partial z} \tag{11c}$$

$$\rho_{21} = A(t,x,z)\frac{dR_0}{dy_2} \tag{11d}$$

where $-A(t,x,z)$ has a simple meaning of the instantaneous displacement thickness. Using (11a,d), the self-induced pressure becomes

$$\frac{\partial p_{24}^{(\kappa)}}{\partial y_2} = -\kappa \frac{dR_0 U_0^2}{dy_2} A(t,x,z) \tag{12}$$

Integration of (12) allows the thermal conditions on the blade surface to be taken into account when evaluating the heat-transfer-coefficient disturbances. The final result implicitly depends on the Mach number involved in the velocity and density distributions, $U_0(y_2)$ and $R_0(y_2)$, across the boundary layer.

Interaction law

As (12) shows, the self-induced pressure oscillations directly relate to the instantaneous displacement thickness $-A(t,x,z)$. The interaction law to connect these two quantities derives from the study of the disturbance pattern in the outer, essentially inviscid sublayer where the normal-to-wall distance is scaled as

$$y^* = \varepsilon^3 L^* y_1 \tag{13}$$

We start again with the asymptotic expansions

$$\frac{u^*}{U_\infty^*} = u_1 = 1 + \varepsilon^2 u_{11}(t,x,y_1,z) + \ldots + \varepsilon^5 u_{14}(t,x,y_1,z) + \ldots \tag{14a}$$

$$\frac{v^*}{U_\infty^*} = v_1 = \varepsilon^2 v_{11}(t,x,y_1,z) + \ldots + \varepsilon^5 v_{14}(t,x,y_1,z) + \ldots \tag{14b}$$

$$\frac{w^*}{U_\infty^*} = w_1 = \varepsilon^2 w_{11}(t,x,y_1,z) + \ldots + \varepsilon^5 w_{14}(t,x,y_1,z) + \ldots \tag{14c}$$

$$\frac{p^* - p_\infty^*}{\rho_\infty^* U_\infty^{*2}} = p_1 = \varepsilon^2 p_{11}(t,x,y_1,z) + \ldots + \varepsilon^5 p_{14}(t,x,y_1,z) + \ldots \tag{14d}$$

$$\frac{\rho^*}{\rho_\infty^*} = \rho_1 = 1 + \varepsilon^2 \rho_{11}(t,x,y_1,z) + \ldots + \varepsilon^5 \rho_{14}(t,x,y_1,z) + \ldots \tag{14e}$$

characteristic of the Tollmien-Schlichting spectral range. In normalized variables

$$\{x,z\} = \left(1 - M_\infty^2\right)^{-\frac{3}{8}} \tau_w^{-\frac{5}{4}} C^{\frac{3}{8}} \left(T_w^*/T_\infty^*\right)^{\frac{3}{2}} \{\hat{x},\hat{z}\} \tag{15a}$$

$$p = \left(1 - M_\infty^2\right)^{-\frac{1}{4}} \tau_w^{\frac{1}{2}} C^{\frac{1}{4}} \hat{p} \tag{15b}$$

$$A = \left(1 - M_\infty^2\right)^{-\frac{1}{8}} \tau_w^{-\frac{3}{4}} C^{\frac{5}{8}} \left(T_w^*/T_\infty^*\right)^{\frac{3}{2}} \hat{A} \tag{15c}$$

the first-order solution

$$p_{11}(t,x,0,z) = -\frac{1}{2\pi}\left(1-M_\infty^2\right)^{-\frac{1}{2}} \int\limits_{-\infty}^{\infty} d\varsigma \int\limits_{-\infty}^{\infty} \frac{\partial^2 A(t,\xi,\varsigma)/\partial\xi^2}{\left[\left(1-M_\infty^2\right)^{-1}(x-\xi)^2 + (z-\varsigma)^2\right]^{\frac{1}{2}}} d\xi \tag{16}$$

incorporating an explicit dependence on the Mach number equally applies to flat as well as curved surfaces. This should be supplemented with a term $\varepsilon^3 p_{14}^{(\kappa)}(t,x,0,z)$ proportional to the surface curvature κ. Making use of the results of the preceding section yields an extended version (Ryzhov, 2001; Ryzhov & Bogdanova-Ryzhova, 2002)

$$\hat{p} = -\frac{1}{2\pi}\left(1-M_\infty^2\right)^{-\frac{1}{2}} \int\limits_{-\infty}^{\infty} d\varsigma \int\limits_{-\infty}^{\infty} \frac{\partial^2 \hat{A}(t,\xi,\varsigma)/\partial\xi^2}{\left[\left(1-M_\infty^2\right)^{-1}(\hat{x}-\xi)^2 + (\hat{z}-\varsigma)^2\right]^{\frac{1}{2}}} d\xi + \varepsilon^3 \kappa D\hat{A} \tag{17a}$$

$$D = \left(1-M_\infty^2\right)^{\frac{1}{8}} \tau_w^{-\frac{5}{4}} C^{\frac{3}{8}} \left(T_w^*/T_\infty^*\right)^{\frac{3}{2}} \tag{17b}$$

of the interaction law where M_∞ and

$$S = \kappa\, \mathbf{Re}^{-\frac{3}{8}} D \tag{18}$$

are two similarity parameters. It is worth noting that the generalized interaction law consists of two components. The first term on the right-hand side of (17a) is associated with the Tollmien-Schlichting waves, the second one relates to the spiral-type Görtler vortices induced by centrifugal forces. Thus (17a,b) stem from the interaction of the wave and vortex eigenmodes evolving on the concave pressure side of a turbine blade.

Final formulation

The interaction law (17a,b) defines both components $\partial\hat{p}/\partial\hat{x}$ and $\partial\hat{p}/\partial\hat{z}$ of the pressure gradient in the Prandtl equations

$$\frac{\partial\hat{u}}{\partial\hat{x}} + \frac{\partial\hat{v}}{\partial\hat{y}} + \frac{\partial\hat{w}}{\partial\hat{z}} = 0 \tag{19a}$$

$$\frac{\partial\hat{u}}{\partial\hat{t}} + \hat{u}\frac{\partial\hat{u}}{\partial\hat{x}} + \hat{v}\frac{\partial\hat{u}}{\partial\hat{y}} + \hat{w}\frac{\partial\hat{u}}{\partial\hat{z}} = -\frac{\partial\hat{p}}{\partial\hat{x}} + \frac{\partial^2\hat{u}}{\partial\hat{y}^2} \tag{19b}$$

$$\frac{\partial\hat{w}}{\partial\hat{t}} + \hat{u}\frac{\partial\hat{w}}{\partial\hat{x}} + \hat{v}\frac{\partial\hat{w}}{\partial\hat{y}} + \hat{w}\frac{\partial\hat{w}}{\partial\hat{z}} = -\frac{\partial\hat{p}}{\partial\hat{z}} + \frac{\partial^2\hat{w}}{\partial\hat{y}^2} \tag{19c}$$

ensuing from the system of original Navier-Stokes equations in the viscous near-wall sublayer. This is a crucial simplification of the problem in the framework of the asymptotic high-Reynolds number formulation based on rescaled normalized variables

$$\frac{t^*}{L^*/U^*_\infty} = \varepsilon^2\left(1- M^2_\infty\right)^{-\frac{1}{4}}\tau_w^{-\frac{3}{2}}C^{\frac{1}{4}}\left(T^*_w/T^*_\infty\right)\hat{t} \tag{20a}$$

$$\frac{y^*}{L^*} = \varepsilon^5\left(1- M^2_\infty\right)^{-\frac{1}{8}}\tau_w^{-\frac{3}{4}}C^{\frac{5}{8}}\left(T^*_w/T^*_\infty\right)^{\frac{3}{2}}\hat{y} \tag{20b}$$

$$\left\{\frac{u^*}{U^*_\infty},\frac{w^*}{U^*_\infty}\right\} = \varepsilon\left(1- M^2_\infty\right)^{-\frac{1}{8}}\tau_w^{\frac{1}{4}}C^{\frac{1}{8}}\left(T^*_w/T^*_\infty\right)^{\frac{1}{2}}\{\hat{u},\hat{w}\} \tag{20c}$$

$$\frac{v^*}{U^*_\infty} = \varepsilon^3\left(1- M^2_\infty\right)^{\frac{1}{8}}\tau_w^{\frac{3}{4}}C^{\frac{3}{8}}\left(T^*_w/T^*_\infty\right)^{\frac{1}{2}}\hat{v} \tag{20d}$$

the notation being standard. The interaction law preserves the ellipticity of the original Navier-Stokes equations which brings about upstream influence. Mathematically, it is just this property which underlies absolute instability in the streamwise direction. The limit conditions

$$\hat{u}- \hat{y} \to \hat{A}(\hat{t},\hat{x},\hat{z}), \quad \frac{\partial \hat{w}}{\partial \hat{x}} \to -\frac{1}{\hat{y}}\frac{\partial \hat{p}}{\partial \hat{z}} \quad \text{as} \quad \hat{y} \to \infty \tag{21a,b}$$

complete the asymptotic formulation for $\mathbf{Re} \gg 1$.

A comparison of classical and interactive approaches

The Görtler number defined in (2) gives the similarity parameter for incompressible flow in the scope of classical hydrodynamic stability theory. The skin friction τ_w varies along the vortex length. The interactive boundary layer scheme predicts a different similarity parameter

$$S = \kappa\, \mathbf{Re}^{-\frac{3}{8}}\left(1- M^2_\infty\right)^{\frac{1}{8}}\tau_w^{-\frac{5}{4}}C^{\frac{3}{8}}\left(T^*_w/T^*_\infty\right)^{\frac{3}{2}} \tag{22}$$

depending on $\kappa\, \mathbf{Re}^{-\frac{3}{8}}$ rather than $\kappa\, \mathbf{Re}$ and involving a combination of the Mach number M_∞, characteristic skin friction τ_w, Chapman viscosity constant C and temperature ratio T^*_w/T^*_∞. All these additional parameters should be considered separately in the classical approach rendering computed results hardly conceivable. Thus, both the scaling and similarity parameters prove to be quite different. Hence, the unsteady spiral-type vortices are not an extension of the classical Görtler vortex structures, rather they are of a mixed wave / vortex character deriving from the Tollmien- Schlichting eigenmode spectrum.

Linear approximation

The theory exposed describes essentially nonlinear motion. When turning to stability problems, we may linearize the system of governing equations by putting

$$\left(\hat{u} - \hat{y}, \hat{v}, \hat{w}, \hat{p}, \hat{A}\right) = \sigma\left(\tilde{u}, \tilde{v}, \tilde{w}, \tilde{p}, \tilde{A}\right) \tag{23}$$

and applying the Laplace-double Fourier transform

$$\left[\bar{u}_c(\omega, k, y, m), \ldots, \bar{A}_c(\omega, k, m)\right]$$

$$= \int\limits_{-\infty}^{\infty} d\hat{x} \int\limits_{-\infty}^{\infty} d\hat{z} \int\limits_{0}^{\infty} e^{-(\omega\hat{t} + ik\hat{x} + im\hat{z})} \left[\tilde{u}(\hat{t}, \hat{x}, \hat{y}, \hat{z}), \ldots, \tilde{A}(\hat{t}, \hat{x}, \hat{z})\right] d\hat{t} \tag{24}$$

Upon solving the system of resulting ordinary differential equations the dispersion relation (Ryzhov, 2001; Ryzhov & Bogdanova-Ryzhova, 2002)

$$\Phi(\Omega) = Q\left(k, m; M_\infty, \varepsilon^3 \kappa D\right), \quad \Omega = i^{-\frac{2}{3}} \omega\, k^{-\frac{2}{3}} \tag{25a,b}$$

to connect the frequency ω with two wavenumbers k, m comes into play. Here

$$\Phi(\Omega) = \frac{dAi(\Omega)}{dY}\left[I(\Omega)\right]^{-1} \tag{26}$$

is a standard function depending on the first derivative $dAi(\Omega)/dY$ and an improper integral

$$I(\Omega) = \int\limits_{\Omega}^{\infty} Ai(Y)\, dY \tag{27}$$

of the Airy function $Ai(Y)$. The arguments of

$$Q = i^{\frac{1}{3}} \frac{k^2 + m^2}{k^{\frac{5}{3}}} \left\{ \frac{k^2}{\left[k^2 + \left(1 - M_\infty^2\right)^{-1} m^2\right]^{\frac{1}{2}}} + \varepsilon^3 \kappa D \right\} \tag{28}$$

are expressed through both wavenumbers and do not contain the frequency.

Spectral side band

The dispersion relation (25a,b) is cast in the form based on the scaling intrinsic to the Tollmien-Schlichting wave spectrum. However, the two terms in curled brackets on the right-hand side of (28) are of different nature. While the first term is associated with

8

the wave motion and gives leading-order contribution, the second term originates from the curvature effects and brings $O(\varepsilon^3)$-correction in the Tollmien-Schlichting range of spectrum. Evidently, a side band of frequencies and wavenumbers should emerge from the interaction of the wave and vortex eigenmodes where they would exert an equal impact on the disturbance pattern. This requirement defines the spectral interval

$$\omega = \varepsilon^{\frac{6}{7}}(\kappa D)^{\frac{2}{7}}\omega_G = \mathbf{Re}^{-\frac{3}{28}}(\kappa D)^{\frac{2}{7}}\omega_G \approx 0.25\omega_G \tag{29a}$$

$$k = \varepsilon^{\frac{9}{7}}(\kappa D)^{\frac{3}{7}}k_G = \mathbf{Re}^{-\frac{9}{56}}(\kappa D)^{\frac{3}{7}}k_G \approx 0.12k_G \tag{29b}$$

$$m = \varepsilon^{-\frac{3}{7}}(\kappa D)^{-\frac{1}{7}}m_G = \mathbf{Re}^{\frac{3}{56}}(\kappa D)^{-\frac{1}{7}}m_G \approx 2.0m_G \tag{29c}$$

of the spiral-type Görtler vortices for typical transition conditions in an incompressible boundary layer with $\mathbf{Re} \sim 5 \cdot 10^5$.

The auxiliary variable Ω and, hence, $\Phi(\Omega)$ are invariants and the affine transformation (29a-c) but Q and D change to

$$Q_G = i^{\frac{1}{3}}\frac{D_G k_G^2 + m_G^2}{k_G^{\frac{5}{3}}}\left\{\frac{k_G^2}{\left[D_G k_G^2 + (1 - M_\infty^2)^{-1}m_G^2\right]^{\frac{1}{2}}} + 1\right\} \tag{30a}$$

$$D_G = \mathbf{Re}^{-\frac{3}{7}}(\kappa D)^{\frac{8}{7}} \tag{30b}$$

with both terms in curled brackets on the right-hand side of (30a) becoming of equal order in magnitude. Thus, in accord with the above conjecture a low-frequency side band comes about from the wave / vortex interaction.

Group velocities

The centrifugal force effects on the overall system of pulsations can be perceived from a comparison of the first dispersion curves in the plane of complex frequencies. Figure 4 drawn with positive values of k is typical of the subsonic boundary layer on a flat plate. The first dispersion curve consists of a single lobe starting at infinity as $k \to \infty$ and terminating in the origin with $k \to 0$. The shape of the first dispersion curves in the plane of complex Görtler frequencies shown in Figure 5 for $m_G = 0.5$ and three values of the Mach number is different. The formation of two lobes connected through a small loop on top is a common feature of all three plots. On theoretical grounds, the prediction of the behavior of disturbances associated with the unusual two-lobe shape of the first

dispersion curve leans upon the general physical concept of the group velocity (Landau & Lifshitz, 1959). The location of the global and local maxima of the real part $\Re\left(\omega_{Gl}\right)$ of the complex frequency in the ω_G-plane is of special significance. The global maximum of $\Re\left(\omega_{Gl}\right)$ on the right-hand lobe, a counterpart of that in Figure 4, is responsible for the generation of short-scaled oscillation cycles in the wave packet sweeping downstream. The wave packets of this type underlie the conventional road to transition provoked by convective instability. A tiny positive peak of $\Re\left(\omega_{Gl}\right)$ in the upper portion of the loops in the shape of the first dispersion curves in Figure 5 is endowed with a negative value of the group velocity. As a consequence, this peak induces a wave packet consisting of much longer oscillation cycles and capable of advancing upstream of a site where the disturbance was given birth.

Absolute instability in the streamwise direction

Thus, the upstream moving modulated signals are brought about by the interaction of the Tollmien-Schlichting wave and G rtler vortex eigenmodes. Centrifugal forces create vortical disturbance structures elongated, in keeping with (29b,c), in the streamwise direction. The surface curvature provides support to centrifugal forces which become zero if a flat plate is under consideration. The Blasius boundary layer mostly studied both theoretically and experimentally so far experiences no wave / vortex interaction and shows no absolute instability in the streamwise direction. However, the first evidence of upstream influence exerted by the vortical disturbances from a concave insert mounted on an otherwise flat plate can be traced back to remarkable wind-tunnel tests by Mangalam, Dagenhart, Hepner & Meyers (1985).

One feature of the first dispersion curves in Figure 5 is worth noting beforehand to obtain reliable results from computations. The size of tiny positive peaks of $\Re\left(\omega_{Gl}\right)$ in the upper portion of the loops in the shape of these curves is much less compared to the magnitude of the global maximum of $\Re\left(\omega_{Gl}\right)$ positioned on the right-hand lobes. Hence a need for filtering out the high-frequency oscillation cycles becomes obvious if both the downstream moving highly-modulated signal and the upstream-advancing wave packet are intended to be computed simultaneously. The plots in Figures 6,7 are drawn using this numerical technique. They correspond to two dispersion curves in Figure 5, one for an incompressible boundary layer and the other for a boundary layer in the high subsonic Mach number regime. The upstream propagating pulsations predicted above theoretically solely from the notion of the negative group velocity are clearly seen in both plots. The frequency of pulsations grows with the Mach number increasing. The absolute instability in the streamwise direction may provoke earlier transition to turbulence.

Conclusions

The present study leads to the following conclusions:

- Unsteady spiral-type Görtler vortices make up a low-frequency side band in the Tollmien-Schlichting wave spectrum.
- Absolute instability in the streamwise direction provoked by the wave / vortex interaction is inherent in any low Mach number as well as high Mach number subsonic boundary layers.
- Filtering out the high-frequency oscillation cycles is required to compute simultaneously the wave packets moving downstream as well as advancing upstream, against the oncoming flow.

Future work: thermal problem

Temperature disturbances remained mostly beyond the scope of traditional hydrodynamic stability. However, understanding the reasons for the heat transfer coefficient to increase is of prime importance in the turbine blade design. This provides a strong impetus to extent the stability analysis to thermal wave packets propagating upstream. The complex-valued amplitude of the forced temperature pulsations introduced in much the same way as in (23) and (24) obeys an inhomogeneous Airy equation

$$\frac{d^2 \overline{T}_c}{dY^2} - Y\overline{T}_c = i^{-\frac{2}{3}} k^{-\frac{2}{3}} \overline{v}_c \qquad (31)$$

subject to the limit condition

$$\overline{T}_c \rightarrow \overline{A}_c \text{ as } |Y| \rightarrow \infty \qquad (32)$$

at the upper reaches of the viscous near-wall sublayer and the boundary condition

$$\overline{T}_c = 0 \text{ at } Y = \Omega \qquad (33)$$

at the solid surface held at constant temperature. Here $\overline{v}_c$ stands for the normal-to-wall velocity component coming from the above solution for the viscous near-wall sublayer. A transformation to the Görtler spectral range

$$\overline{v}_c = \varepsilon^{\frac{3}{7}}(\kappa D)^{\frac{1}{7}} \overline{v}_{cG}, \quad \overline{T}_c = \varepsilon^{-\frac{3}{7}}(\kappa D)^{-\frac{1}{7}} \overline{T}_{cG} \qquad (34)$$

preserves the boundary-value problem intact.

Some recent results based on a solution to this problem are submitted by Bogdanova-Ryzhova & Ryzhov to ASME Turbo EXPO 2003. As it follows from (31), the temperature oscillations in the upstream moving wave packets may have even larger

amplitude than the normal-to-wall velocity (and pressure) if the length of G̅rtler vortices grows without bounds as $k_G \to 0$.

References

Choudhari M., Hall P. & Streett C. **1994**. On the spatial evolution of long-wavelength G̅rtler vortices governed by a viscous / inviscid interaction. Part 1: The linear case. *Q. J. Mech. Appl. Maths.*, **47**, 207-229.

Denier J. P., Hall P.& Seddougui S. O. **1991**. On the receptivity problem for G̅rtler vortices: vortex motions induced by wall roughness. *Phil. Trans. R. Soc. London*, **A355**, 51-85.

Landau L. D. & Lifshitz E. M. **1959**. Fluid Mechanics. Pergamon.

Mangalam S. M., Dagenhart J. R., Hepner T. E. & Meyers J. F. **1985**. The G̅rtler instability on an airfoil. *AIAA Paper 85-0491*.

Saric W. S. **1994**. G̅rtler vortices. *Ann. Rev. Fluid Mech.*, **26**, 379-409.

Smith F. T. **1979**. On the non-parallel flow stability of the Blasius boundary layer. *Proc. R. Soc. London*, **A358**, 3091-3111.

Zhuk V. I. & Ryzhov O.S. **1980.** Free interaction and stability of a boundary layer in incompressible fluid. Sov. Phys. Dokl., **25**, 577-579.

Interactions

- An invited lecture: Boundary layer instabilities in transonic range of velocities. IUTAM Symposium Transsonicum IV. G̅ttingen, Germany. September 2002 (jointly with E. V. Bogdanova-Ryzhova).
- A lecture: The G̅rtler instabilities in a subsonic boundary layer. Dept. of Mechanical & Aeronautical Engineering, University of California, Davis, October 2002.

Transitions

- A letter in support of the activities on investigations within this grant is sent to Air Force Office of Scientific Research from PS, GE.
- The work on boundary-layer instabilities in transonic range of velocities is done jointly with Dr. E. V. Bogdanova-Ryzhova (GE, Global Research Center).

Publications

Ryzhov O. S. 2001 Advances in hydrodynamic stability theory: the wave / vortex eigenmodes' interaction. Numerical Simulations of Incompressible Flows. World Scientific.

Ryzhov O. S. & Bogdanova-Ryzhova E. V. 2002. Boundary layer instabilities in transonic range of velocities. Proceedings of the IUTAM Symposium IV. Kluwer Academic

Bogdanova-Ryzhova E. V. & Ryzhov O. S. 2003. Heat transfer induced by wave / vortex eigenmodes' interaction. ASME TURBO EXPO 2003 (submitted).
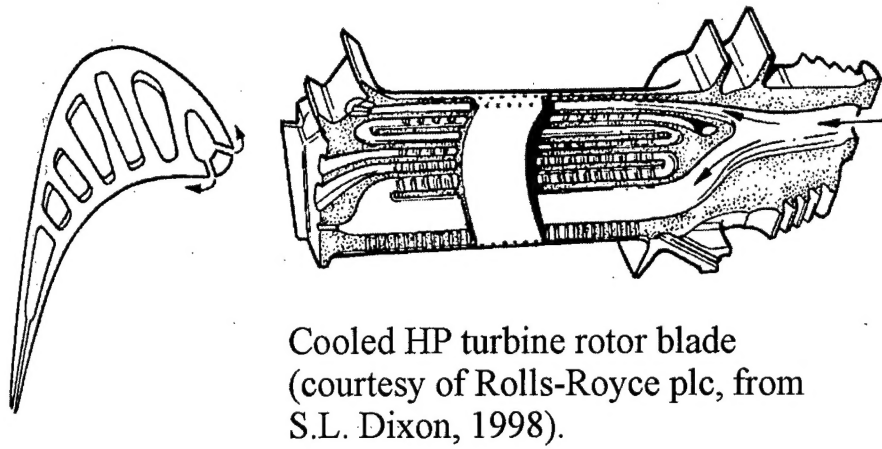
Cooled HP turbine rotor blade
(courtesy of Rolls-Royce plc, from
S.L. Dixon, 1998).

Figure 1. Typical shape of a turbine blade.

Sketch of the streamwise vortices developing on a
concave wall due to the Görtler instability mechanism.
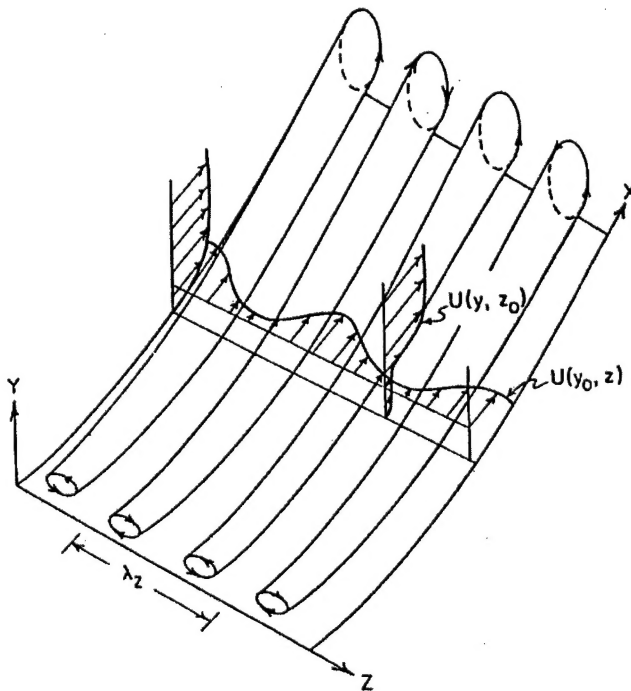
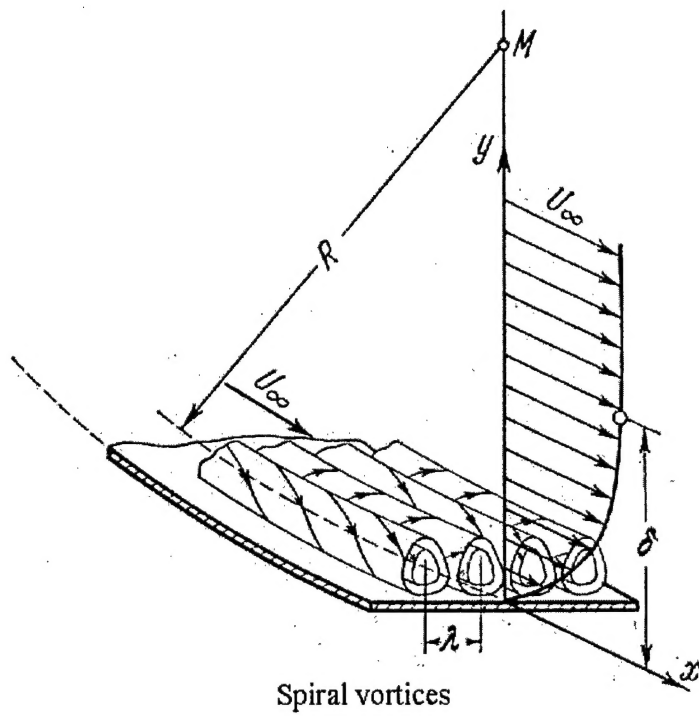Figure 2. Steady vortical disturbances in the classical boundary layer.

14

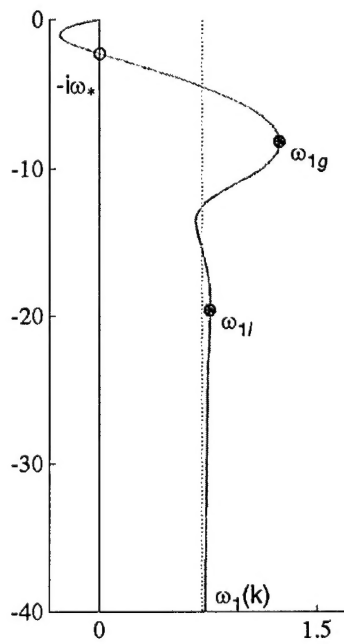Figure 3. Unsteady vortical disturbances in an interactive boundary layer.

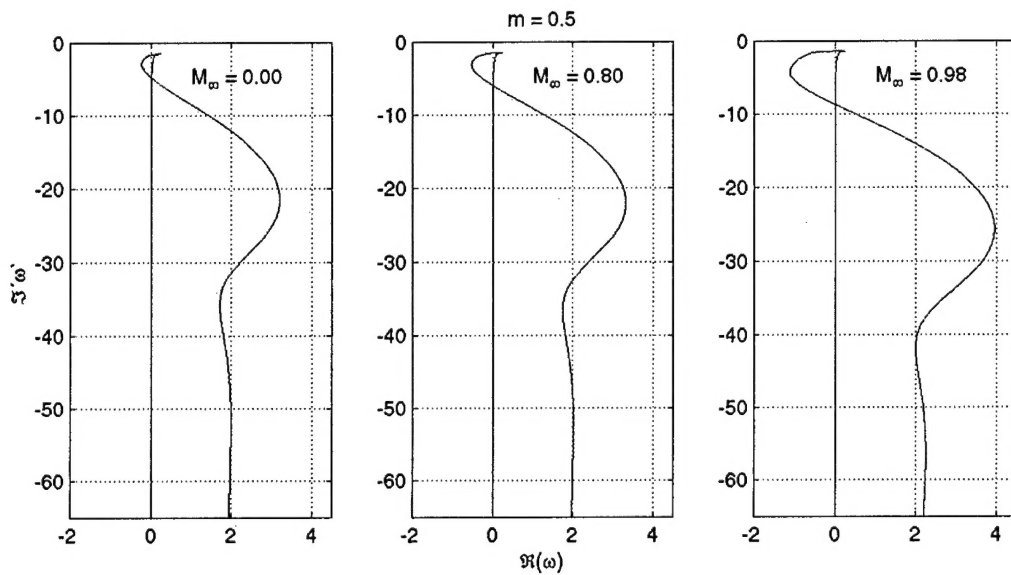Figure 4. Complex frequencies for incompressible boundary layer.

m = 0.5

Figure 5. Complex frequencies for compressible boundary layers in different subsonic regimes.
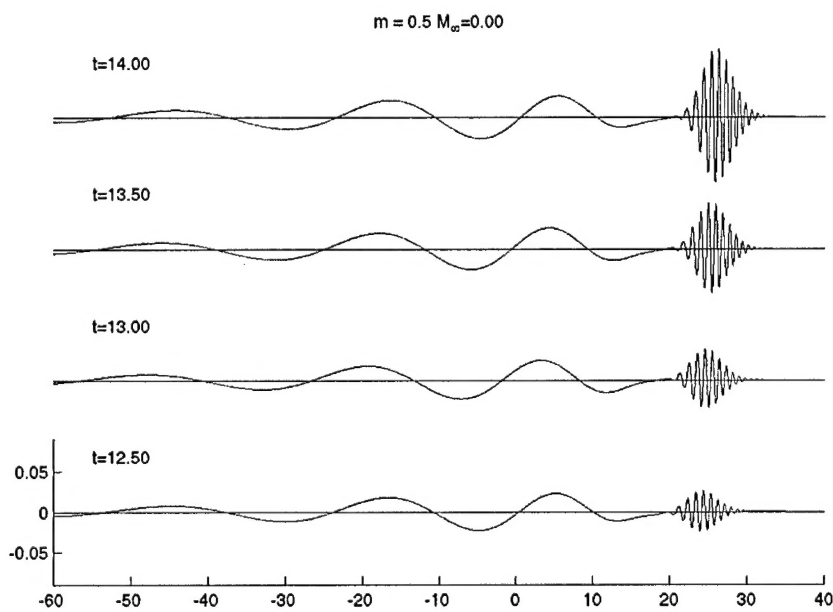
m = 0.5 M∞=0.00

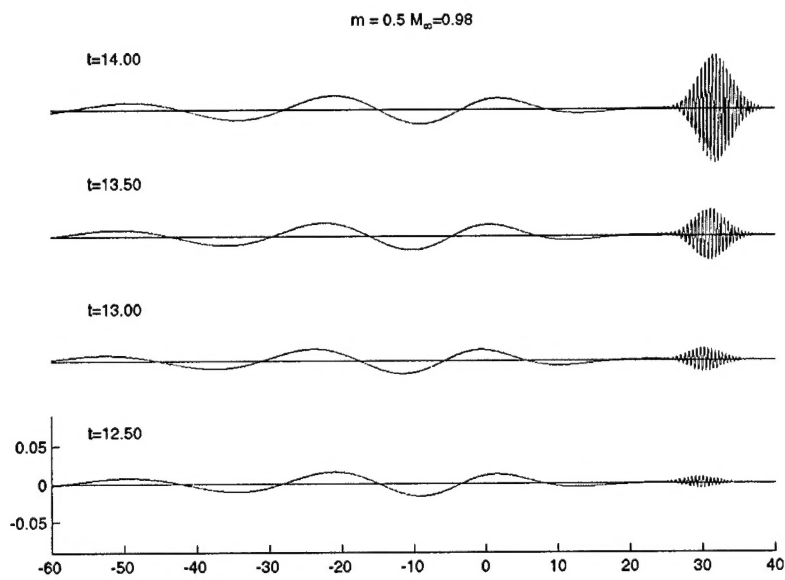Figure 6. Downstream and upstream propagating disturbances in an incompressible boundary layer.

Figure 7. Downstream and upstream propagating disturbances in compressible boundary layer in the high subsonic Mach number regime.